# Improving SeaSonde Radial Velocity Accuracy and Variance using Radial Metrics

Tony de Paolo and Eric Terrill
Coastal Observing Research and Development Center
Scripps Institution of Oceanography
La Jolla, California, USA
tdepaolo@ucsd.edu

Anthony Kirincich
Woods Hole Oceanographic Institution
Woods Hole, Massachusetts, USA
akirincich@whoi.edu

***Abstract*— The surface current observations made by HF radar systems are increasingly being relied on to support decision-making by coastal ocean users and managers. Thus, the need for high quality data with defined error characteristics has never been higher. Building on previous efforts, this paper examines the use of 'radial metrics', the ancillary output of the direction finding algorithm used by the SeaSonde radar system, to improve both accuracy and error characterization. The radial metrics provide non-velocity based parameters that can be used to eliminate low-quality data and or weight the contribution of individual returns on the resulting spatially averaged radial velocity. While their effects on the data are different, both thresholding and weighted averaging based on the metrics are shown here to significantly increase the accuracy and reduce the error of the resulting velocity estimates. Thus, we suggest that operators should take advantage of these advancements to improve the accuracy of existing systems.**

**Keywords—HF Radar; ocean currents**

## I. INTRODUCTION

Land-based high frequency (HF) radar systems are increasingly being employed for determining surface currents in the near-shore ocean environment. As of 2014, there were 130 radars operating in the United States alone as part of a collective coastal ocean observatory sponsored by the U.S. Integrated Ocean Observing System (IOOS). Owned and maintained by more than 30 institutions, the data from these systems are provided in real time to more than 40 government/private entities to support marine domain awareness and operational decision making. Given the increasing reliance on 'environmental intelligence' by these and other coastal ocean stakeholders, the need for high quality observations with known, standardized error characteristics has never been greater. This work investigates the potential for increasing surface current accuracies and reducing variances via the use of non-velocity metrics associated with the ancillary data output of commonly deployed radar systems.

The most common radar used in the U.S. system is the SeaSonde, produced by CODAR Ocean Sensors (COS). The SeaSonde is a direction-finding radar which uses a compact array of three co-located antennas. The complex signal voltages from each of the three antennas are used with a direction-finding algorithm (Multiple Signal Classification (MUSIC),[1]) to find the direction of arrival (DOA) function for each observed velocity [2]. Peak value(s) of the DOA function give the estimated bearing of the signal(s), with a maximum of two bearings allowed by the three-antenna array. All velocity estimates at a given range having bearings within a 5-degree wide azimuthal angle are averaged to estimate the radial velocity reported for each range/azimuthal bin.

The abilities of these algorithms to resolve the bearing of surface current signals are well documented [2-6], and a number of previous works have examine the potential quality of the SeaSonde surface current data [7-10]. In practice, these works have shown that errors, as rms differences from in situ sensors, can vary widely (6-30 cm $s^{-1}$) depending on the characteristics of the site and radar. Noise levels of 4-6 cm $s^{-1}$, driven by both instrument noise and sub-grid scale current variability, have been inferred from these and other comparisons [7, 10-12].

A smaller number of works [13-15] have focused on relating non-velocity signal quality metrics, the ancillary results of the MUSIC direction-finding system, to the total accuracy of the surface current estimates. Thus, the values of these parameters, can be related to the quality of individual radial velocity estimates and, potentially, used to improve the overall accuracy of the resulting radial surface currents. Following these initial works, we further explore the use of radial current velocity metrics to improve current estimates.

Thus, this work documents the potential for error reduction in SeaSonde radial velocities via using the radial metrics to screen or weight the raw radial estimates. Error reduction will be quantified using observations collected at two separate systems of 25-Mhz SeaSonde radars: one system existing off Martha's Vineyard, Massachusetts, and a second off Southern California. These systems are focused on here due to the existence of collocated in situ velocity estimates for comparison or substantial along-baseline comparisons between individual radars. After an introduction to Radial Metrics and the datasets being utilized, we examine the role of screening the data based on thresholds and the effect they have on the velocity results. This will be done using both in situ

978-1-4799-8736-8/15/$31.00 ©2015 IEEE

sensors and along baseline comparisons to examine the potential for error reduction and its time dependence. Additionally, the ability of spatial averages of the radial velocity that are weighted by the radial metrics, as a quality indicator, to offer further error reduction is quantified before our conclusions are offered.

## II. SeaSonde Radial Metrics

The analysis described here utilizes the Radial Metric output of CODAR Ocean System's version 7 release of the SeaSonde Radial Site Software Suite to examine both the characteristics of the received signal and the output of the direction-finding algorithm. These ancillary outputs from the direction-finding step of the standard processing protocol of the SeaSonde have the potential to offer estimates of the quality of the radial velocity estimates that are independent of the velocities themselves. Previous studies [13-14] have identified the six MUSIC parameters/metrics from the SeaSonde Radial Metrics files that offer the most potential benefits as quality indicators. Listed here, along with the exact names given to them in the Radial Metrics file, they are:

1. Maximum value of the Direction of Arrival (DOA) function
    a. MusicSngl Peak Resp
    b. MusicDual Peak1Resp
    c. MusicDual Peak2Resp
2. Width of the DOA function
    a. MusicSngl Pk Width
    b. MusicDual Pk1 Width
    c. MusicDual Pk2 Width
3. Signal Power
    a. MusicSngl Pwr (dB)
    b. MusicDual Pwr1 (dB)
    c. MusicDual Pwr2 (dB)
4. Doppler Cell Signal to Noise Ratio (SNR) from Antenna 1
    a. SpectraA1 S/N (dB)
5. Doppler Cell SNR from Antenna 2
    a. SpectraA2 S/N (dB)
6. Doppler Cell SNR from Antenna 3
    a. SpectraA3 S/N (dB)

The definition of these parameters is given in [14]. For each radial velocity produced, a set of these values are provided within the SeaSonde Radial Metric files.

To use these metrics to provide information on the quality of the velocity itself, one must first determine what constitutes a value that might indicate a low quality velocity estimate. The quality of a metric value is assumed here to be a function of its location in a probability density function of the metric for that file. For example, a histogram of SNR from Antenna 3 is given in Fig. 1.

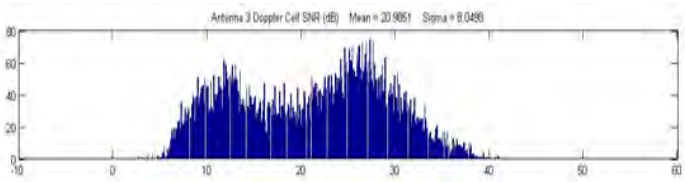

Fig. 1 – Histogram of SNR from Antenna 3 for one radial metric data file (one hour) from the SIO SDCI site.

These values are logarithmic, with a mean of 20.1 dB, and a standard deviation of 8.0 dB. Certainly high SNR is good, so we focus on the part of the histogram that exhibits low SNR. As an example of the filtering scheme used here, we may remove radial velocity vectors that are 2 standard deviations below the mean, and see if that improves baseline radial velocity consistency by a reduction of component variance. In previous works [13-14], all combinations of the six metrics listed above were examined for their potential to provide the needed information on the quality of the velocity data. Additionally, [13] also varied the filter threshold through values of [0 0.5 1.0 1.5 2.0 2.5 3.0]. These efforts found that low values of the Signal Power and SNR from Antenna 3, metrics 3 and 6 described earlier, were the most closely linked to suspect velocity output from MUSIC. Both a high Signal Power and a high SNR 3 are favorable, and typically produce more accurate radials. Thus, the use of these two parameters to screen the data represents the starting point for the present work.

## III. Data and Methods

### *A. Martha's Vineyard, Massachusetts*

A system of three 25 MHz SeaSonde HF radars, operating in the coastal ocean south of the island of Martha's Vineyard, Massachusetts will be used to validate use of filtering, or thresholding, the velocity results based on the Radial Metric output. Maintained by Woods Hole Oceanographic Institution (WHOI) and first described in [15], this system was reconfigured in 2014 to focus on surface currents over a wider coastal area in connection with a research study funded by the U.S. National Science Foundation. In addition to expanding and operating the HF radar system, this project deployed five bottom-mounted, upward-looking acoustic Doppler current profilers (ADCPs) at water depths of 15, 20, or 25 m for up to a 6-month period in 2014 (Fig. 2). Data from an additional bottom-mounted ADCP, operated and maintained by WHOI's Martha's Vineyard Coastal Observatory and located in 12-m of water at a cabled, underwater node, is also included in the analysis. Each of these sensors is located within the coverage area of the HF radars at ranges from 5 to 20 km offshore.

The 30 day period of November 2014 is chosen for analysis here to focus consideration only during times most likely to have weaker stratification and thus, less stratification-driven velocity shear between the effective measurement depth of the 25 MHz HF radar, ~0.25 m, and the near-surface ADCP-based velocity, generally 2-3 m below. A similar product to the CODAR Radial Metric-type of data files is available for each of the radars for the period of the in situ deployments. For the WHOI HF radar system data set is based on fully independent estimates of the Radial Metrics every 15 minutes.

The ADCP to HF radar comparisons are prepared following [15]. The nearest HF radar radial average grid point to each ADCP location was chosen as the point of comparison. The 30-min ensemble averaged ADCP results from the surface-most bin were rotated into a coordinate system aligned with the bearing to radar site in question and temporally averaged to hourly values, as was the 15 min radial averages. Finally, an estimate of the total Stokes drift at the effective depth of the radar observations was subtracted from the HFR surface current time series to account for this difference between the two observations [18]. ADCP-based estimates of the significant wave height, dominant wave period, and significant wave direction, calculated by MVCO using standard analysis methods from the 12-m ADCP observations, were used to estimate the Stokes drift present at the radar's effective depth using linear wave theory. Previous results [15] have shown that comparisons not accounting for this difference can increase the rms differences between the measurements by 1 to 1.5 cm $s^{-1}$, depending on the water depth and wave climate.

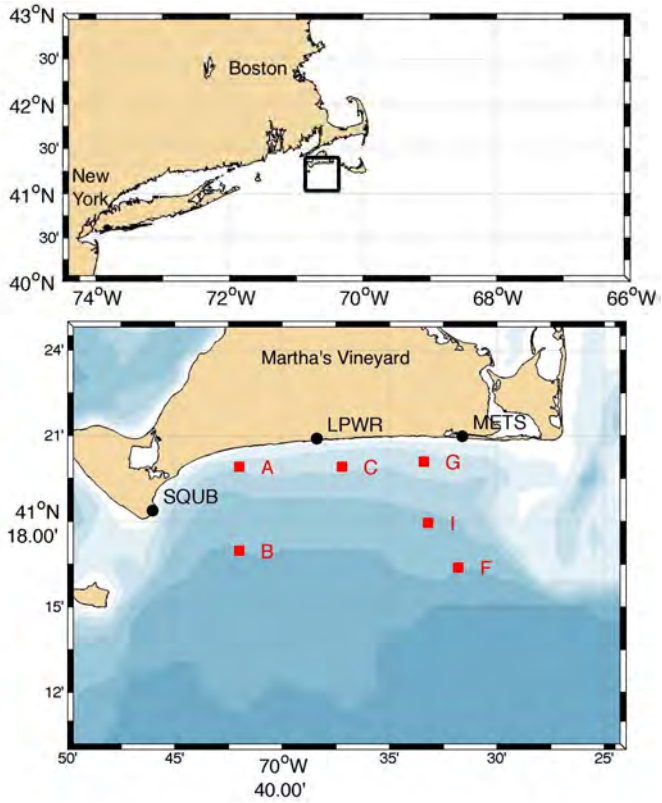


Fig. 2 (Top) Southern New England with the WHOI study area shown in the box. (Bottom) The WHOI study area south of Martha's Vineyard with the locations of the WHOI radars, in black, and moorings, in red.

### B. Southern California

The Scripps Institution of Oceanography (SIO) Coastal Observing Research and Development Center (CORDC) operates a system of three 25 MHz SeaSonde systems off the coast of San Diego, CA. These systems are some of the most long running HF radars contributing data to the U.S. network and have been utilized in multiple works on local and regional dynamics [16, 17]. Importantly, the relative placement of the radar sites: Point Loma (SDPL), Border Park (SDBP), and Coronado Island (SDCI) offers substantial areas of open water that are along the baseline between pairs of radars. Thus, in these areas, the radial velocities from overlapping systems are directly comparable.

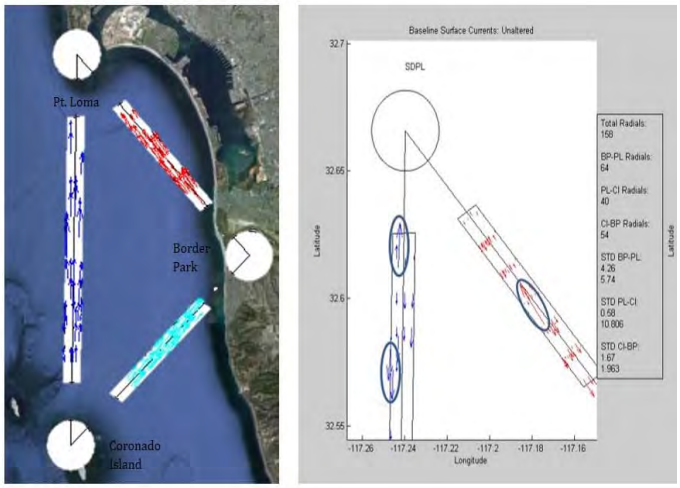


Fig. 3 – CORDC SeaSonde system layout, baselines identified, and inconsistent vectors circled

The baseline regions of the CORDC SeaSonde system are shown in Fig. 3, as are some sample radial velocity vectors. The analysis of radials along the baseline region allows 'inconsistent data' to be easily identified. Circled within the right hand panel, one can see the inconsistent radial velocity vectors going the opposite direction from the general flow. In addition, some vectors in the correct direction are too large in magnitude.

In this analysis, forty-five days of data from the year 2008 were used, and days with higher than average wind speeds were typically selected. For this time period, the CORDC systems' Radial Metric output was gathered and hourly averages of the dataset were used to examine both the histograms of the Radial Metrics and the radial velocities themselves. While the full data files were used to determine the mean and standard deviation of the metrics, only the results of radials that fell in the baselines of the station pairs are shown in the results described below.

## IV. Analysis and Results

### A. Martha's Vineyard, Massachusetts

#### 1) Defining Optimum Threshold Levels

The multiple in situ comparative observations available within the WHOI dataset allow us to demonstrate the relative change in accuracy (as rms differences against the top bin of the ADCPs) as well as the reduction in the variance of the radial average. Secondly, the variations in location of the ADCPs relative to each HF radar sites allow us to examine the results both for how well the metrics work to reduce errors as well as,

TABLE 1. The five versions of dynamic thresholding cutoffs compared along with a sixth run using no thresholds or the COS standard processing.

| Run | Signal Power | Antenna 3 SNR |
|---|---|---|
| 1 | μ - 1.5 σ | μ - 2.0 σ |
| 2 | μ - 2.0 σ | μ - 1.5 σ |
| 3 | μ - 1.5 σ | μ - 1.5 σ |
| 4 | μ - 1.0 σ | μ - 1.5 σ |
| 5 | μ - 2.0 σ | μ - 1.0 σ |
| 6 | no thresholding | no thresholding |

importantly, where in the domain of a typical HF radar system these types of thresholds are likely to have the biggest impact on increasing the overall accuracy and variance of the remotely sensed estimates of surface currents.

For each 15-min observation of the Radial Metrics, thresholds for signal power and antenna 3 SNR are used to screen the Radial Metric output used to estimate the 15-min spatial average of the radial velocities. Five versions of the dynamic thresholding cutoffs (Table 1) are compared to the COS processing suite standard results (i.e. no thresholding) to quantify the potential for error reduction. Both the adjusted HF radar and ADCP radial velocity timeseries at the location of each ADCP are time averaged to independent 1-hr intervals for the comparisons shown. Variance estimates from the independent HF radar estimates were also averaged to the same 1-hr time interval.

For all six ADCP sites, the results are shown in Fig. 4, for the rms differences, and Fig. 5 for the radial velocity variances. In both figures, the results for all runs for each radar at each ADCP location are connected by solid lines to clearly show the change in rms difference due to the different combination of thresholds applied. Results for onshore sites, shown on the top panels, generally have higher levels of overall rms difference and variance than offshore locations. In general, among the 5 different thresholding levels considered here, thresholds with more restrictive cutting (particularly run 4) make gains in accuracy and variance reduction. However, all make improvements, albeit sometimes incremental, on the existing COS methods, i.e. run 6.

The gains in accuracy and variance for the most restrictive thresholds are more apparent for an individual radar as the bearing from the radar to the point of comparison/location approaches the orientation of the shoreline itself. These are generally the onshore sites, given the geometry of the WHOI array and the location of the ADCPs (Fig. 3). This likely occurs as signals returning from these highly oblique incidence angles tend to be lower in power and higher in noise. Thus, the use of thresholds in these areas of lower returning signal power makes a bigger impact on lowering the error rates and variances.

This increase in accuracy appears to come without any noticeable reduction in performance, as the radial average timeseries at each of the in situ locations have similar amounts of gaps or missing radial averages over the 30 day period considered (not shown here). Thus, for these 25 MHz systems, sufficient data exists, even after eliminating as much 10-15% of the raw radials to allow nearly complete radial averages time series.

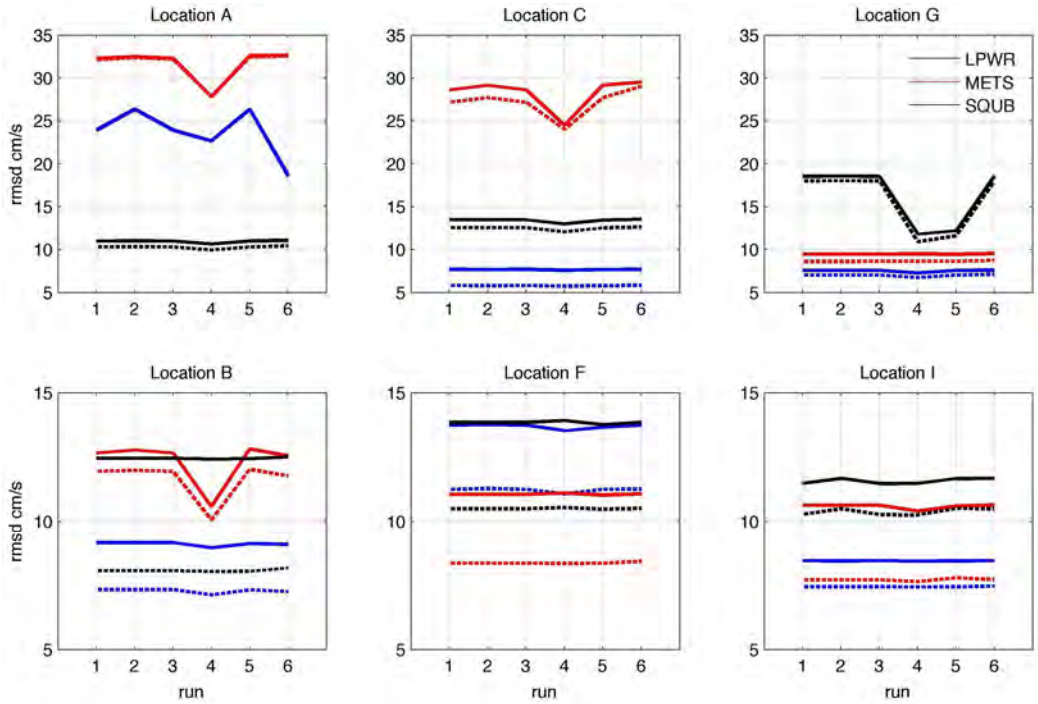


Fig.4 – WHOI HF radar rms differences between the radial velocities of each radar and the ADCP velocities at each site for each of the threshold runs defined in Table 1 (solid) without, and (dashed) with the additional signal power weighted averaging described by [15]. Onshore sites (A, C, and G) are shown in the top panels, while offshore sites (B, F, and I) are shown in the bottom panels. Note differences in scales for the top and bottom rows.

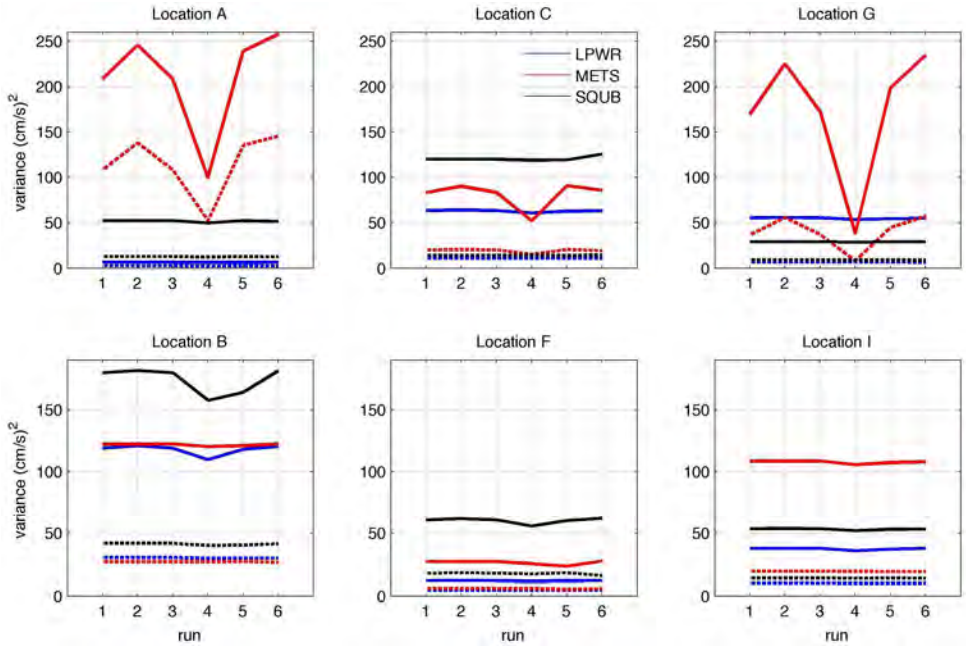

Fig. 5—Same as 5, but for the radar estimated variance. Note differences in scales for the top and bottom rows.

*2) The Role of Weighted Averaging*

In addition to the use of threshold values for the radial metrics to reduce velocity errors, [15] also examined the application of a weighing function on the raw radial data used to compute the average radial velocity for each range and azimuthal bin. As described by [15], weighting the radials by the signal power itself was found to reduce rms differences against ADCP observations in addition to the reductions gained by thresholding. However, the work of [15] only considered the application of static, low level (i.e. SNR > 5 dB) thresholds. Thus, the ability of this weighting function to provide additional gains in accuracy for the range of dynamic thresholds considered here is of great interest.

The resulting radial averages using the five dynamic thresholds described above were recomputed with the additional use of the weighting function to estimate a new radial average and variance for each threshold pair. The weight, defined as

$$w(i)=v(i)/\Sigma v(i)$$

where $v$ is the signal power in volts for each of $i$ radial velocity estimates falling within the range/azimuthal bin considered and $\Sigma$ denotes a summation, is used to define the power-weighted radial average as

$$r = \Sigma\, d(i)w(i)$$

where $d$ is the raw radial estimate for each i radial velocity estimate passing the threshold test. The weighted variance then follows as

$$\Sigma w(i)[(d(i)-r]^2.$$

Justification for the use of the signal power as weight is as follows. Assuming that the wind forcing over an individual range/azimuthal cell is constant, or nearly constant, a radial velocity estimate having a true signal power larger than that of a second radial from the same range/azimuthal cell can be interpreted as being more representative of the true surface velocity over the cell's area. Physically, this can be thought of as more of the cell `moving' at the first velocity, leading to a stronger return from the cell at that velocity.

Using the 30-day dataset of HF radar and ADCP velocities collected by WHOI, estimates of the radial average velocity that use both thresholds and signal power weighted averaging were made for all threshold pairs are shown in Table 1. Using these additional estimates of the radar-based radial velocities, the radar to ADCP comparisons were recomputed for all radar and ADCP location combinations and are shown in Figs. 4 and 5 by dashed lines.

At the majority of the combinations of ADCP locations and radar sites, the rms differences associated with the power-weighted averages are noticeably less than those of either the COS standard or thresholding-only results. This reduction is anywhere from 2 to 5 cm/s in reduced rms difference, leading to substantial gains particularly at the offshore sites considered (B, F, and I in Fig. 4). In a small number of comparisons, the dashed lines are not visible as they overlie the solid lines that describe the thresholding-only results. These situations occur when the thresholding-only rms differences and variances are quite high (i.e. location A for radars METS and LPWR), suggesting that, when the radar results are seriously degraded,

weighted averaging offers no measureable benefit towards reducing the observed rms differences.

The addition of the power-weighted averaging also offers substantial reductions in the variance about the spatial average (Fig. 5). Note, however, that the variance is computed as a power-weighted variance as defined above. The reductions in variance present even when there are still significant rms differences between the radar and ADCP-based estimates of the radial velocity (i.e. locations G or A) are consistent with previous results [7-9, 12, 15] showing that real differences both between the two measurement types being compared here as well as in the top few meters of the water column, all else being equal. Regardless, these comparisons illustrate that use of the power-weighted averaging offers a significant reduction in the rms difference from the ADCP or the radial variance itself. The additional component of weighted averaging is able to reduce accuracy and/or variance at all locations, regardless of the incident angle, making it useful throughout the entire domain of the radar.

## *B. Southern California*

### *1) Temporal Dependence of Variance Reduction*

With the previous results in mind, data from the CORDC system off Southern California are used to examine the temporal dependence of the potential variance reduction. Following the above results, a threshold of 1.5 sigma below the mean values for each hour of the Signal Power and Antenna 3 SNR metrics was used to filter out low quality data. Using these threshold pairs, Fig. 6 shows a typical result for three days between Border Park and Pt. Loma. During the time periods highlighted by the red boxes, one can see clear reductions in variance due to the filtering of the velocity data by the radial metrics. Figure 7 shows the same for the baseline between Coronado Island and Pt. Loma. It should also be noted that not all baselines will behave the same way

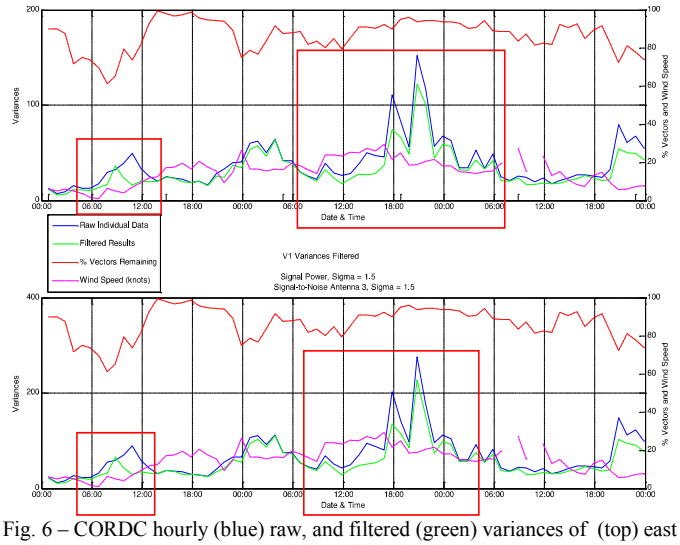


Fig. 6 – CORDC hourly (blue) raw, and filtered (green) variances of (top) east and (bottom) north components of the radial velocities between sites SDPL and SDBP for 72 hours. The percentage of vectors remaining after filtering is also shown in red as is the wind speed in magenta on each panel.

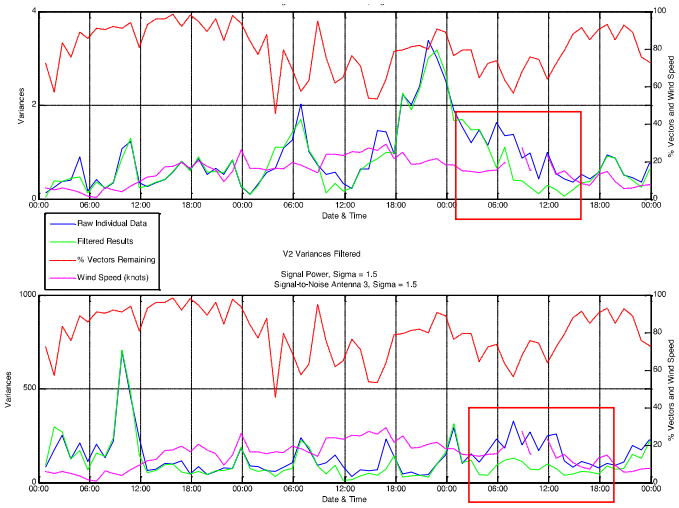


Fig. 7 – Same as Fig. 6 but for the SDCI to SDPL baseline.

with respect to choice of thresholds due to the location of the baseline within the individual radars coverage area, as shown above. For example, on the Border Park to Coronado baseline (Fig. 8), the number of radials removed in this area was consistently much lower than that of the other two baselines as this baseline had higher signal power and SNR.

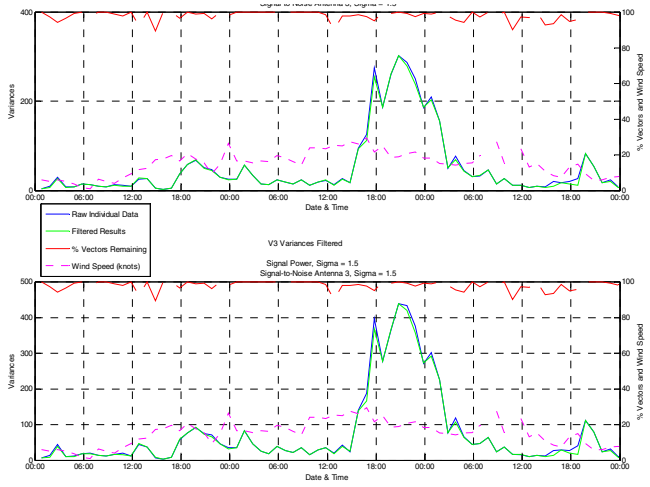


Fig. 8 – Same as fig. 6 but for the SDBP to SDCI Baseline

To condense the previous graphs over multiple three day periods, data was analyzed each hour over each three day period and then averaged to allow for the readjustment of the radial metric distributions each hour. The improvement in variance of the data set was analyzed in 3 ways:

### *a) Percentage of hourly variances improved*

Using our filtering scheme, either the baseline variance went down (improved), remained the same, or went up. As shown in the top panel of Fig. 9, the percentage of the hours that the baseline variance improved over each three day period, in the three day period between 12/20/07 – 12/22/07 (the dark blue bar), the hourly baseline variance improved 65% of the time.

In this case the baseline variance remained the same 25% of the time, and increased 10% of the time.

*b) Average percentage of vectors removed*

Each hour, the number of radial velocity vectors that were removed were counted, and the percentage of the total number of vectors was calculated. The middle panel of Fig. 9 shows the average percentage of radial velocity vectors removed over each three day period. For example, for the three day period between 12/20/07 – 12/22/07 (dark blue bar), 11.5% of the vectors were removed. This has the effect of a slight reduction in geographic coverage, however with improved vector variance.

*c) Average variance improvement per vector removed*

Finally, as a kind of "bang for your buck" measurement, the bottom panel of Fig. 9 shows the average variance improvement per vector removed (what we fondly refer to as the "Nager Number"). Note that this is NOT the ratio of the previous two graphs, as they were given as percentages, but an absolute measurement of variance reduction divided by the number of vectors removed.

After conducting the analysis and graphing the results it has still somewhat subjective to pinpoint a best filtering method for any given system. By applying a "heavier" filter, more data is thrown away and the variance is improved by a significant amount. But in some cases this can result in eliminating 20% of the original data. By applying a "lighter" filter, less data is thrown away and the Nager Number is improved. In order to select a best filtering method it may be helpful to set thresholds on what percentage of data being removed the individual SeaSonde operator can accept. However, these results coupled with those found in figs. 6-8 clearly illustrate that histograms of the metrics change with the oceanic and atmospheric conditions (wind speed and direction, tide, etc.) present. Therefore, computing probability density functions on short time scales, i.e. the hourly or shorter scales used here, is warranted.

*2) Drivers of Residual Errors*

Even after filtering the data, a number of radials remained that could be classified as inconsistent with the mean radial for that location. In the most obvious cases, these were radials that opposed the general direction of the current along a given baseline. In order to determine a method to filter out these remaining outliers, the six radial metrics listed above, along with the bearing of the radial and an additional metric denoting whether the radial was the result of a single or dual angle solution, were examined to further understand the characteristics of inconsistent radials. For this analysis we chose one three day period from the CORDC data set, and found the following:

a) all vectors prior to filtering
b) inconsistent vectors prior to filtering
c) all vectors after filtering
d) inconsistent vectors after filtering

The following criteria were established for defining inconsistent vectors:

a) the mean current must have a magnitude of at least 3 cm/s
b) inconsistent vectors pointed in a direction that was opposite to the mean direction
c) inconsistent vectors must have a magnitude of at least 1 cm/s

This last criteria exists as, in cases were the surface current has a relatively small magnitude it is not completely unreasonable to see two current directions in one baseline.

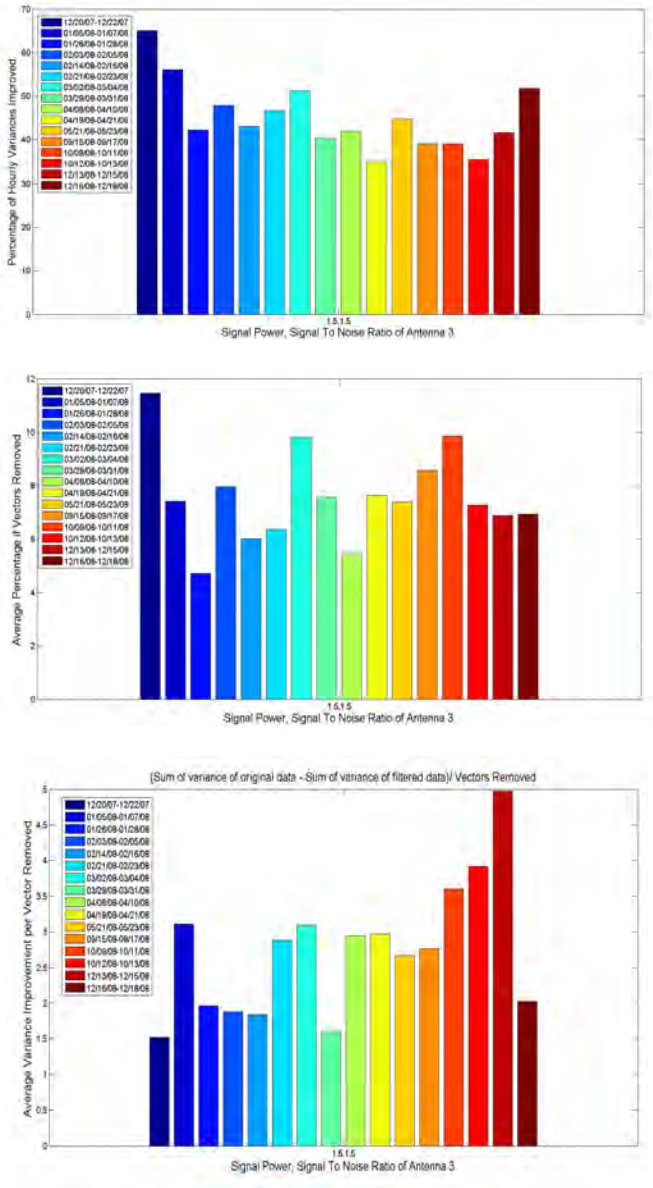


Fig. 9 – Results of CORDC 3-day averages of the filtered baseline variances in terms of the (top) percentage of hourly variances improved, (middle) the average percentage of vectors removed, and (bottom) the average variance improvement per vector removed (Nager Number).

For the single verses dual angle solution metric, a value of either 10, for single bearings, or 20, for dual bearings, was assigned to each radial estimate before the average was computed. Thus, an average value near 20 would mean that

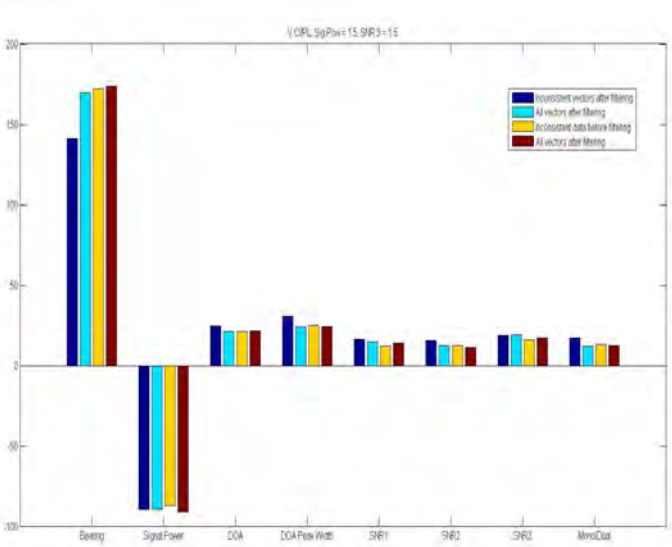

Fig. 10 – Characteristics of inconsistent radials for a 3-day period along the SDCI to SDPL basline. Units for all parameters are dB except for Bearing and DOA peak width (degrees), and MonoDual (see text).

the remaining inconsistent radials tended to be from dual angle solutions, while an average value near 10 would mean that the remaining inconsistent radials tended to be from single bearing solutions.

Results for a 3-day period along the SDCI to SDPL baseline (Fig. 10) which are representative of the results from the full dataset, reveal three important qualities of the inconsistent radials that remain after filtering. First, as seen from the difference in bearing between the inconsistent radials and either the filtered or raw radials, inconsistent data found along the baseline appeared to have a different bearing than 'consistent' data. This can very clearly be seen in the Fig. 10 Bearing bar chart. The dark blue bar shows the remaining vectors to come from a different bearing. This is merely an artifact of our data processing and should not be considered significant by the reader. Secondly and more importantly, as shown by the change in the Mono/Dual ratio, it appears that inconsistent vectors remaining after filtering are dominated by dual angle results. In almost all cases the remaining inconsistent data is made up of 80-95% dual angle results. Thirdly, the results for the DOA Peak Width illustrate that inconsistent results tend to have wider DOA functions. These last two conclusions have also been shown in previous results [13], where the second maximum in the DOA function is ill defined (low value, large width) and produces low quality results.

From these results, we infer that the DOA peak width might also be an important metric to filter the data in order to improve the accuracy of the current in the baselines. While this was also found by [15], it appears that the 'wide' values in the present analysis originated from the second, lower peak of the dual angle solutions. As shown by [15], it was wide peaks associated by single angle solutions that were most eliminated by thresholding based on this metric. Finally, the results of this analysis also show that a number of metrics, including DOA peak values, SNR1 values and SNR2 values given similar results between any of the averages considered. Thus, none of these metrics would be useful for filtering out the remaining inconsistent radials.

## V. Conclusions

We have long been proponents of using the ancillary output of the MUSIC algorithm, i.e. the Radial Metrics file output of the SeaSonde Radial Software Suite, to improve the accuracy and quality of SeaSonde output. The method presented here: (1) targeted filtering of the raw radial velocity estimates prior to the calculation of the spatially averaged radials and (2) signal-power weighted spatial averaging of the raw estimates has been shown to increase the accuracy and reduce the variance of radial velocities associated with SeaSonde HF radar systems.

The level of error and variance reductions found here are consistent with [15], which considered a much smaller set of radar to ADCP comparisons. Thus, these results offer the strongest proof to date of the potential gains in HF radar performance by using a combination of Radial Metric thresholds and power-weighted radial averaging. These improvements come at the expense of only a slight, if noticeable, reduction in coverage. Again, the methodology can be applied to all radial directions, not just along baselines between sites or at locations of in situ comparisons.

Now that the Radial Metrics output is available with every new SeaSonde system, and via an upgrade for older systems, we encourage SeaSonde operators to incorporate use of these metrics in their operational systems. Given our extensive efforts, which have determined that Signal Power and Antenna 3 SNR provide the best quality indicators for the 25 MHz systems described here, we suggest using these metrics and the thresholds described above as a starting point. However, it might be useful to analyze the results in a similar manner to that described above in order to determine if different metrics and/or thresholds might be appropriate for HF radar systems with different characteristics (i.e. operating frequency, oceanic conditions, etc.). Comparison to in-situ sensors (ADCPs) or baseline variance analysis provides an easy measure of the potential system's increase in consistency and quality, as would comparisons to drifter trajectories as well.

Finally, we note that additional work examining the DOA Peak Width metric, and the use of Dual Angle solutions

appears warranted. These metrics are related, as it is often the case that the second dual angle solution has a wider DOA Peak Width. Additionally, based on the utility of weighted spatial averaging in reducing radial errors shown here, we suggest that a related system of quality weights could be applied to the total or vector velocities computed using the radials from multiple sites. Future work should also work to associate an overall quality metric with each radial velocity vector, which will be used to weight individual radial velocity vectors in the computation of the total system vectors using multiple sites.

## ACKNOWLEDGMENT

We wish to thank CODAR Ocean Sensors for their continuing cooperation and support of our efforts. The Southern California work was sponsored by the US National Oceanographic and Atmospheric Administration (NOAA) US Integrated Ocean Observing System (IOOS) Program Office, Jack Harlan Ph.D. Project Manager, HF Radar Ocean Remote Sensing. Additionally, Tony de Paolo and Eric Terrill wish to thank current and former members of CORDC including Sean Celona, Tom Cook, Lisa Hazard, Andy Nager, and Jacob Teal. The Martha's Vineyard work was sponsored by internal WHOI funding and NSF Award OCE-1332646. Anthony Kirincich wishes to thank Steve Lentz, Ben Hodges, and MVCO for their help in creating and maintaining the WHOI HF radar system.

## REFERENCES

[1] Schmidt, R., "Multiple emitter location and signal parameter estimation," IEEE Trans. Antenna Propagation, Vol. 34, No. 3, pp. 276–280, 1986.

[2] Lipa, B., Nyden, B., Ullman, D., Terrill, E., "SeaSonde radial velocities: derivation and internal consistency", IEEE Journal of Oceanic Engineering, Vol. 31, No. 4, October 2006.

[3] Barrick, D. E. and B. J. Lipa, "Correcting for distorted antenna patterns in codar ocean surface measurements" IEEE J. Oceanic Eng., Vol. 11, No. 2, pp. 304–309, 1986.

[4] Barrick, D. E. and B. J. Lipa, "Evolution of bearing determination in HF current mapping radars" Oceanography, Vol. 10, pp. 72–75, 1997.

[5] Kohut, J. and S. Glenn, "Improving HF radar surface current measurements with measured antenna beam patterns," J. Atmos. Oceanic Technol., Vol. 20, pp. 1303–1316, 2003.

[6] Paduan, J., K. Kim, M. Cook, and F. Chavez, "Calibration and validation of direction- finding high frequency radar ocean surface current observations," IEEE J. Oceanic Eng., Vol. 31, No. 4, pp. 862-875, 2006.

[7] Emery, B., L. Washburn, and J. Harlan, "Evaluating radial current measurements from CODAR high-frequency radars with moored current meters," J. Atmos. Oceanic Technol., Vol. 21, No. 8, pp. 1259–1271, 2004.

[8] Ullman, D. and D. Codiga, "Seasonal variation of a coastal jet in the Long Island Sound outflow region based on HF radar and Doppler current observations," J. Geophys. Res., Vol. 109, No. C07S06, doi:10.1029/2002JC001 660, 2004.

[9] Kohut, J., H. Roarty, and S. Glenn, "Characterizing observed environmental variability with HF Doppler radar surface current mappers and acoustic Doppler current profilers: Environmental variability in the coastal ocean," IEEE J. Oceanic Eng., Vol. 31, doi:10. 1109/JOE.2006.886 095, 2006.

[10] Ohlmann, C., P. White, L. Washburn, E. Terrill, B. Emery, and M. Otero, "Interpretation of coastal HF radar–derived surface currents with high-resolution drifter data," J. Atmos. Ocean Technol., Vol. 24, No. 4, pp. 666-680, 2007.

[11] Rypina, I. I., A. R. Kirincich, R. Limeburner, and I. Udovydchenkov, "Eulerian and lagrangian correspondence of high-frequency radar and surface drifter data: effects of radar resolution and flow components," J. Atmos. Oceanic Technol., Vol. 31, No. 4, pp. 945–966, 2014.

[12] Hubbard, M., D. Barrick, N. Garfield, J. Pettigrew, C. Ohlmann, and M. Gough, "A new method for estimating high-frequency radar error using data from central San Francisco Bay," Ocean Sci. J., Vol. 48, No. 1, 2013.

[13] de Paolo, T., Terrill, E., "Skill assessment of resolving ocean surface current structure using compact-antenna-style HF radar and the MUSIC direction-finding algorithm", J. Atmos. Oceanic Technol.,. 24, No. 7, July 2007.

[14] de Paolo, T., Terrill, E., "Properties of HF radar compact antenna arrays and their effect on the MUSIC algorithm", Scripps Institution of Oceanography eScholarship Publications, http://escholarship.org/, November 2007.

[15] Kirincich, A., de Paolo, T., Terrill, E., "Improving HF radar estimates of surface currents using signal quality metrics with application to the MVCO high-resolution radar system", Journal of Atmospheric and Oceanographic Technology, Vol. 29, September 2012.

[16] Kim, S., E. Terrill, and B. Cornuelle, "Objectively mapping HF radar-derived surface current data using measured and idealized data covariance matrices," J. Geophys. Res., Vol. 112, No. C06021, 2007.

[17] Kim, S., "Observations of submesoscale eddies using high-frequency radar-derived kinematic and dynamic quantities.," Cont. Shelf Res., Vol. 30, No. 15, pp. 1639–1655, 2010.

[18] Creamer, D., F. Henyey, R. Schult, and J. Wright, "Improved linear representation of ocean surface waves," J. Fluid Mech., Vol. 205, pp. 135–161, 1989.